CLIMATOLOGY

Higher probability of compound flooding from precipitation and storm surge in Europe under anthropogenic climate change

E. Bevacqua[1]*[†], D. Maraun[1], M. I. Vousdoukas[2,3], E. Voukouvalas[4], M. Vrac[5], L. Mentaschi[2], M. Widmann[6]

In low-lying coastal areas, the co-occurrence of high sea level and precipitation resulting in large runoff may cause compound flooding (CF). When the two hazards interact, the resulting impact can be worse than when they occur individually. Both storm surges and heavy precipitation, as well as their interplay, are likely to change in response to global warming. Despite the CF relevance, a comprehensive hazard assessment beyond individual locations is missing, and no studies have examined CF in the future. Analyzing co-occurring high sea level and heavy precipitation in Europe, we show that the Mediterranean coasts are experiencing the highest CF probability in the present. However, future climate projections show emerging high CF probability along parts of the northern European coast. In several European regions, CF should be considered as a potential hazard aggravating the risk caused by mean sea level rise in the future.

INTRODUCTION

The interaction of high sea level and heavy precipitation may cause compound flooding (CF), a coastal hazard that can result in substantial damages and fatalities (1–4). Prominent examples of CF in Europe are the flash flood in Lisbon, 1967 (5); the Avon flood in Bristol, 2014; and the Ravenna flood in 2015 (3). In 2012, The Netherlands almost experienced a flooding of the water board Noorderzijlvest, which led to precautionary evacuation (6). The recently released pan-European HANZE (Historical Analysis of Natural Hazards in Europe) database (7) lists 24 co-occurrences of storm surges and river floods along the Irish, U.K., Belgian, and Polish coasts, the French Atlantic and Mediterranean coast, and the Italian Adriatic coast. Estimating the coastal flooding risk is essential for policy-making, disaster risk reduction, and engineering practices. At the moment, the CF hazard is usually omitted in coastal flooding risk analyses, implying that sea and river flooding are considered as independent phenomena (2).

However, the meteorological and hydrological processes that drive flooding from land and sea are, to a certain extent, related. The co-occurrence or close succession of a heavy precipitation event and a storm surge is driven by deep low-pressure systems (1, 2). Although heavy precipitation alone can be caused by convection without intense cyclonic activity (8), the latter is also a precondition for storm surges (Fig. 1). Intense cyclones drive storm surges through strong winds pushing water toward the coast and the barometric pressure effect (3, 9). CF can be caused by several mechanisms (2). A storm surge can block or slow down the precipitation drainage into the sea (3), causing flooding along the coast (2, 6). Runoff from a river may require a certain time to drain into the sea such that precipitation may have to occur well before the storm surge. Similarly, flood levels of a storm surge may be amplified by any relevant amount of precipitation (2). Last, a flood may occur when precipitation falls on wet soil that is saturated by a preceding storm surge. The relative importance of these mechanisms in a particular location depends on both the local climate and topography (2), but all of the above implies that storm surges and extreme precipitation runoff are often not independent phenomena. Therefore, ignoring their dependence may substantially underestimate the resulting CF risk (2, 3, 6, 10, 11).

Several studies have demonstrated the importance and damaging nature of CF for selected locations (3, 6, 11, 12). Recently, Ward et al. (13) presented the first assessment of the dependence between observed high sea levels and high river discharge for estuaries around the globe, although the sparse observations precluded the assessment in several regions. Comprehensive studies exist for the United Kingdom (9), Australia (14), and the coastal areas of the United States (U.S.) (2). The U.S. study detected an increasing probability of CF during the past decades, although it was not possible to attribute this increase to anthropogenic climate change. However, given that extreme precipitation (15), river flooding (16), and extreme sea levels (17–19) are expected to increase under future climate change, it is likely that also the CF probability will increase along with these driving processes. Furthermore, coastal cities are expected to further grow in the coming decades (19), and more and more people will be exposed to CF, rendering an analysis of CF in the future urgent. So far, only the effect of mean sea level rise (SLR) on the changing CF hazard has been analyzed and only for selected locations in the U.S. (11). The future CF probability, taking into account future changes of precipitation, storm surges, waves, and astronomical tides, has not yet been assessed.

Against the foregoing background, we analyze the CF hazard along the European coasts both for present and future climate according to the business-as-usual (RCP8.5) scenario. A precise CF hazard probability assessment can, in practice, only be site specific because the actual CF hazard depends strongly on the local interactions between topography, fluvial or pluvial flooding, and ocean (2). Furthermore, the final CF risk estimate also depends on the existing flood protection and the exposed population and assets. Modeling these local details would, however, preclude a continental-scale analysis. Thus, we do not analyze the effective CF, but we limit ourselves to modeling the probability of potential CF, which, for the sake of brevity, we express as CF probability only: We

[1]Wegener Center for Climate and Global Change, University of Graz, Graz, Austria. [2]European Commission, Joint Research Centre, Ispra, Italy. [3]Department of Marine Sciences, University of the Aegean, Mitilene, Greece. [4]S.A. Rue des Deux Eglises 26, Brussels 1000, Belgium. [5]Laboratoire des Sciences du Climat et de l'Environnement, CNRS/IPSL, Gif-sur-Yvette, France. [6]School of Geography, Earth and Environmental Sciences, University of Birmingham, Birmingham, UK.
*Corresponding author. Email: e.bevacqua@reading.ac.uk
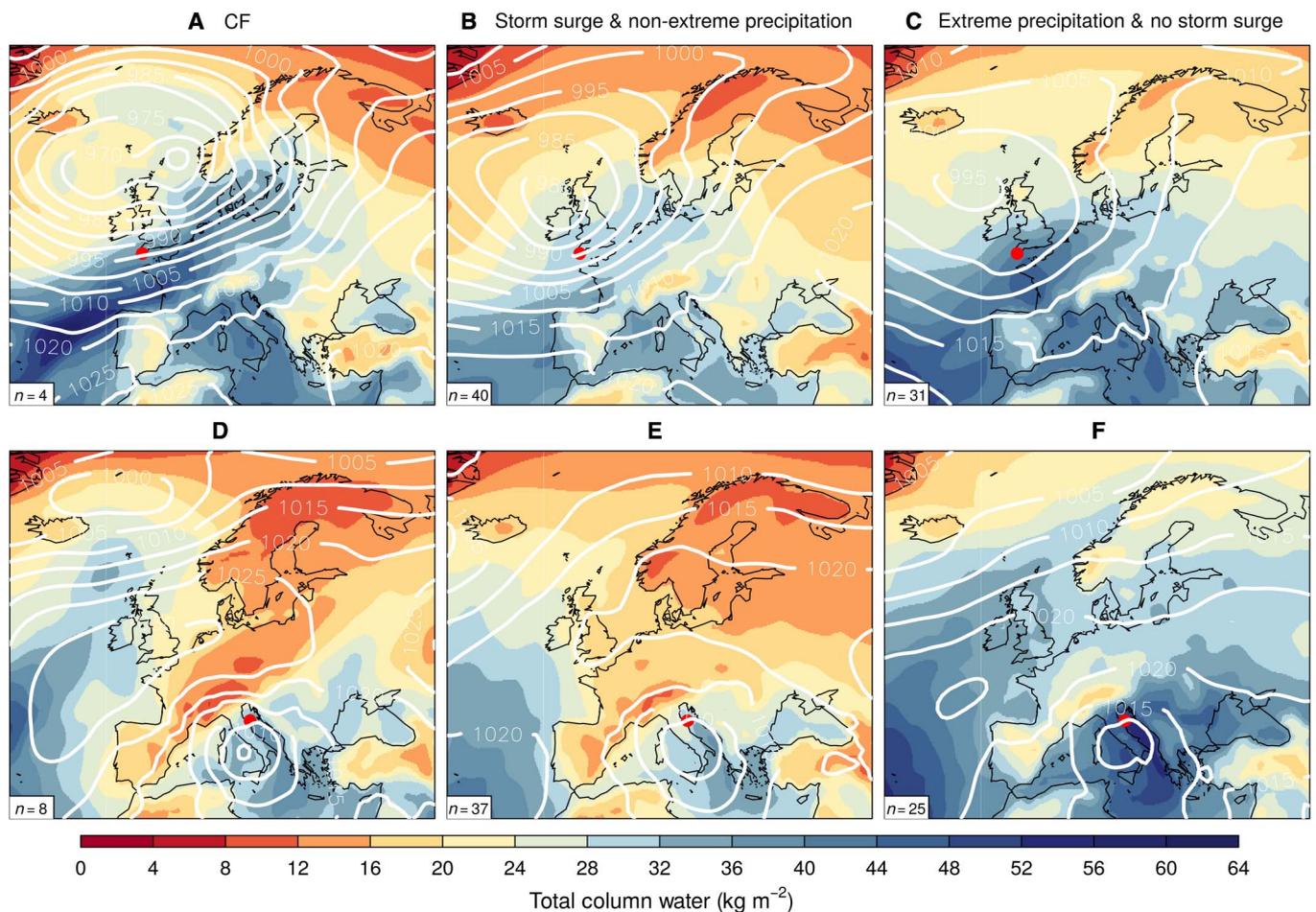†Present address: Department of Meteorology, University of Reading, Reading, UK.

Fig. 1. Synoptic weather conditions driving extreme events. Composite maps of sea level pressure (hPa, in white) and total column water fields computed over days where extreme events (>99.5th percentile) occurred in Plymouth (UK, top) and Ancona (Italy, bottom) indicated by the red dots (based on ERA-Interim data, 1980–2014). Here, the astronomical tide component of the sea level is not considered to focus only on the meteorological-driven part. Extreme events type: (**A** and **D**) compound flooding (CF), (**B** and **E**) storm surge but not extreme precipitation, and (**C** and **F**) extreme precipitation but not storm surge. The total number of extreme events considered for computing the composite maps is shown at the bottom left corner of the panels. Storm surges include the wave setup contribution (see text).

follow the approach of previous studies (2, 13, 18) and model the probability of co-occurring high sea levels and heavy precipitation. Although flooding can also be driven by very extreme sea level or precipitation only, analyzing the probability of their co-occurring high values allows for focusing on CF and understanding their changes. At the end of the 21st century, SLR will be the primary threat for coastal areas (fig. S1) (20), and societies are already aware that, although challenging, they will need to adapt to this impact of climate change by raising dikes, constructing new flood protection, or abandoning coastal areas (11, 18, 19). However, CF may pose an additional hazard beyond mean SLR that has yet to be considered (10). Therefore, for the projections, we focus on the additional CF hazard caused by the meteorological CF drivers, without considering mean SLR.

RESULTS

To characterize extreme sea level, we consider daily maximum values of the superposition of storm surges (including waves) and astronomical tides. In the following, we will refer to these maxima simply as sea level. Storm surges and waves are simulated with the hydrodynamic D-FLOW

Flexible Mesh (FM) (17, 20, 21) and Wavewatch III (17, 20, 22) models, respectively, forced with ERA-Interim reanalysis data (23) for present climate (1979–2014), and with data from six selected Coupled Model Intercomparison Project Phase 5 (CMIP5) models (24) for present (1970–2004) and future climate (2070–2099). Astronomical tides are simulated separately considering the effects of SLR during the century (see Materials and Methods for more details). Precipitation is directly taken from the reanalysis and the six CMIP5 models. On each day, we consider accumulated precipitation within a time range of ±1 days, which allows us to account for precipitation occurring just before and after midnight of the storm surge day (25) and for the mentioned mechanisms responsible for CF. This approach cannot account for CF caused by a storm surge concurring with high river discharge driven by a previous weather system. However, it allows for indirectly considering CF caused by moving weather systems that first cause precipitation further inland around the coast and later a storm surge (see Materials and Methods for a discussion). We define univariate extremes of the individual hazards as events occurring on average every 1 year for sea level and precipitation (fig. S2) (the results are similar to when using 200 days and 5 years as thresholds to define the univariate extremes). We compute the CF return

period (T_{CF}), which is defined here as the average waiting time between the co-occurrence of these extreme events (26) (see Materials and Methods for a discussion on the return period definition). T_{CF} corresponds to the reciprocal of the probability of this co-occurrence (P_{CF}), i.e., $T_{CF} = 1/P_{CF}$; hence, in the following, we will alternatively refer to return periods or probabilities as a low return period corresponds to a high probability and vice versa. We model the dependence of sea level and precipitation extremes by a copula-based multivariate probability model. For details, refer to Materials and Methods, and for an evaluation of the simulated CF probability, see the Supplementary Materials (figs. S3 to S5).

Locations experiencing the highest CF probability in present climate

The highest CF probability in present climate is mainly concentrated along the Mediterranean Sea (Fig. 2). The Atlantic coast appears to be particularly exposed to co-occurring storm surges and extreme precipitation (fig. S6). But here, the effective probability is reduced because of the high tidal range (fig. S6): No CF occurs when the peak of the storm surge coincides with neap tides. In present climate, about 3% of the coastline experiences return periods of CF shorter than 6 years. These regions are the Gulf of Valencia (Spain), the northwestern Algeria, the Gulf of Lion (France), southeastern Italy, the northwest Aegean coast, southern Turkey, and the Levante region (Fig. 2). The statistical dependence between sea level and precipitation greatly enhances the probability of CF along the European coasts: When ignoring the dependence, the CF return period increases by up to two orders of magnitude (365 years is the expected return period in the independent case).

The CF probability in a warmer climate

In a warmer future climate, the probability of CF is projected to robustly increase particularly along the west coast of Great Britain, northern

CF probability (1980–2014)

Fig. 2. Present probability of potential compound flooding (CF). Return periods of CF (co-occurring sea level and precipitation extremes, i.e., larger than the individual 1-year return levels) based on ERA-Interim data.

France, the east and south coast of the North Sea, and the eastern half of the Black Sea (Fig. 3A). The fraction of coastlines experiencing return periods lower than 6 years is projected to increase from presently 3 to 11% by the end of the 21st century. Hot spot regions where return periods will fall below this value are the Bristol Channel and the Devon and Cornwall coast in the United Kingdom, as well as the Dutch and German North Sea coast (Fig. 3B). Along the Noorderzijlvest water board, which also faces the greatest SLR, the model-mean probability of potential CF will triple; the Norwegian West coast around Bergen will see a fivefold increase in potential CF frequency.

The projected increase in CF frequency shows strong statistical significance along the Western British Isles, the North and Baltic Sea (see the projected return periods lying outside the baseline confidence intervals for regions 3, 4, and 5 in Fig. 3C). Along much of the Mediterranean coast, climate models do not agree about the direction of future changes in CF probability; along the Strait of Gibraltar, CF probability is even expected to decrease (Fig. 3A).

Drivers of the CF probability change

Changes in CF probability can, in principle, be caused by changes in the probability of extreme sea levels and extreme precipitation, as well as in the dependence between both hazards (2, 3, 6, 11) (Materials and Methods). For Europe and the Southern Mediterranean, the main driver of future changes in CF probability appears to be changes in precipitation (Fig. 4), as a warmer atmosphere will allow storms to carry more moisture, resulting in heavier precipitation. This thermodynamic effect dominates along the North Atlantic storm track in Northern Europe, and the Mediterranean storm track (15). Weaker upward winds will reverse the thermodynamic increases of extreme precipitation over northwestern Africa (15) (Fig. 4C and fig. S7). For most regions, the considered CMIP5 model ensemble shows poor agreement on changes in the dependence between precipitation and sea levels and, as a result, on the projected sign of changes in CF probability (Fig. 4A). Reducing extreme sea levels cause a CF probability decrease along the Mediterranean coast, while the opposite is projected along the west coast of Great Britain and North Sea, and eastern coast of the Baltic Sea (Fig. 4B and fig. S7).
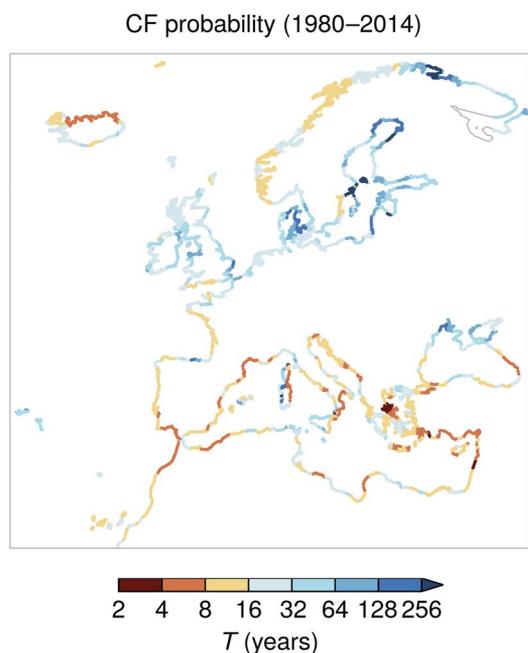
DISCUSSION

This continental study comes with some inevitable limitations mainly related to the resolution of the input data and the omission of the nonlinear interactions between the different physical factors leading to CF; i.e., SLR, astronomical tides, waves, storm surges, precipitation, and hydrology. Coupled modeling of the above could improve the accuracy of the CF assessment but was not feasible given the available computational and storage capabilities. The same applies to the use of higher-resolution forcing data and models, which would improve the representation of precipitation (27), wind, and extreme sea levels (28, 29). Our study analyzed the probability of potential CF, i.e., focusing on the spatiotemporal dynamics of meteorological drivers of flooding. Therefore, our findings cannot directly be interpreted as projections of actual flood risk, since the latter is a complex phenomenon depending on several other factors not presently considered, e.g., the topography and the presence of protection. If a particular site is not prone to surges, e.g., because of the local cliffs, and fluvial or pluvial flooding, the CF hazard may be negligible, although we identified a high potential CF hazard. However, the above shortcomings are common in large-scale studies like the present, which provides a pan-European assessment of the CF hazard in view of climate change.
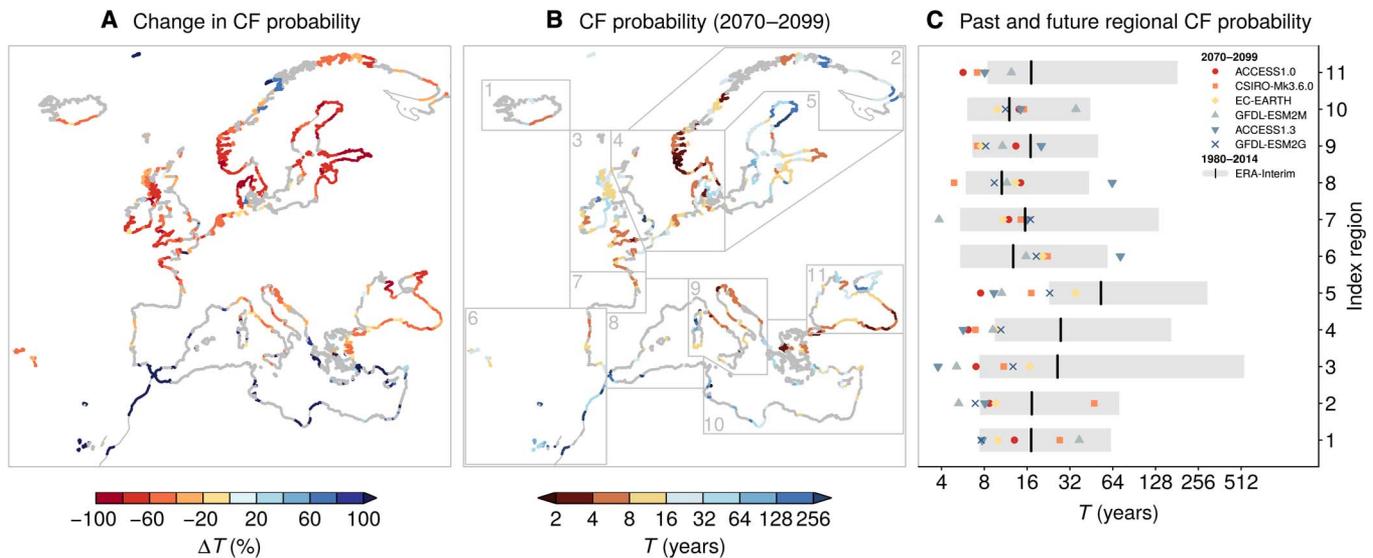
A Change in CF probability   **B** CF probability (2070–2099)   **C** Past and future regional CF probability

Fig. 3. Future probability of potential compound flooding (CF). (**A**) Multimodel mean of projected change (%) of CF return periods, between future (2070–2099) and present (1970–2004) climate. (**B**) Return periods for the future (2070–2099). Gray points indicate locations where only four or fewer of six models agree on the sign of the return period change (three or less of five models in the Black Sea). Areas of gray points in (A) and (B) are slightly different, as the former are computed taking into account the past period (1970–2004) and the latter the period (1980–2004) (see delta change approach in Materials and Methods). (**C**) Median value of CF return periods over regions defined in (B) for past [1980–2014, based on ERA-Interim (Fig. 2)] and future (2070–2099) climate, separately for individual models. For ERA-Interim, gray shading illustrates the sampling uncertainty 95% range.

A Dependence-driven CF probability change   **B** Sea-driven CF probability change   **C** Precipitation-driven CF probability change
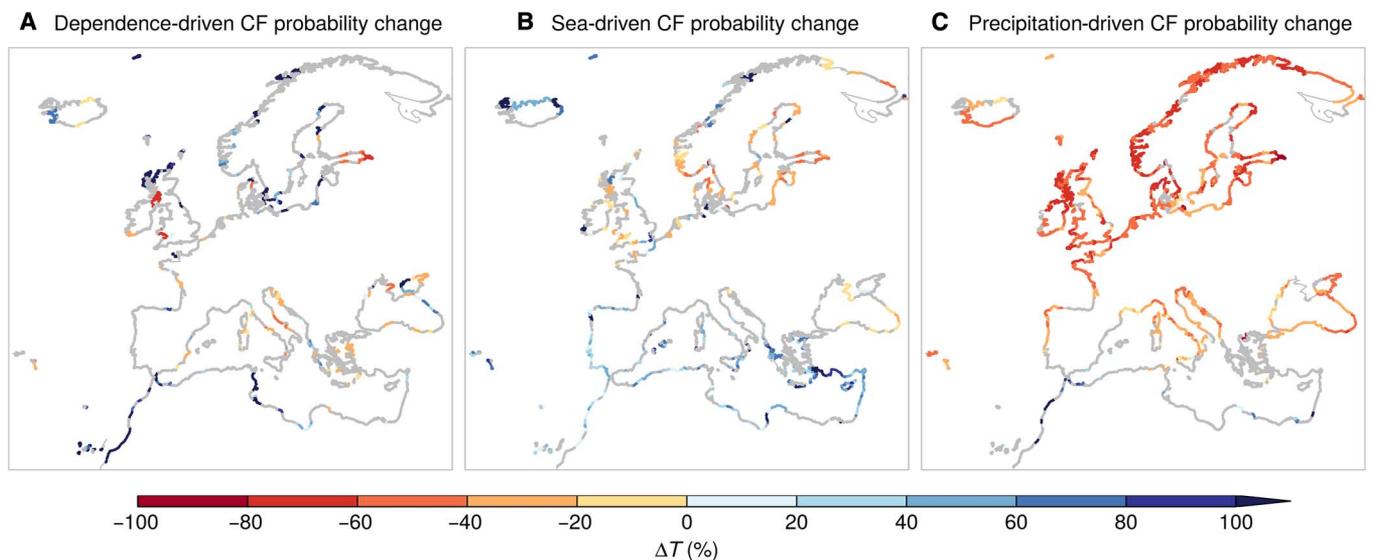
Fig. 4. Attribution of probability change in potential compound flooding (CF) to changes in dependence and marginal distribution. Multimodel mean of projected change (%) of CF return periods between future (2070–2099) and present (1970–2004) when only taking into account future changes of: the overall (**A**) dependence [Spearman and tail dependence (*3*)] between sea level and precipitation, (**B**) sea level distribution, and (**C**) precipitation distribution (Materials and Methods). The total projected probability variation (Fig. 3A) is not given by the sum of these three cases (A, B, and C), as the overall dependencies and marginal distributions do not contribute linearly to the CF return periods. SLR is not considered in the definition of future sea levels (see text). Gray points indicate locations where only four or fewer of six models agree on the sign of the return period change (three or less of five models in the Black Sea).

Rising mean sea levels will pose the main threat along coastal areas in a warmer climate (*20*), and SLR will naturally drive an increase in the co-occurrence of extreme sea level and precipitation (fig. S1B) (*11*, *30*). Coastal planning agencies in Europe are already aware of these changing hazards and the urgency to respond with timely and effective adaptation strategies (*13*, *18*, *19*). Here, we have demonstrated that CF will have substantial additional changes to those

caused by SLR and that the CF hazard should be taken into account for a complete present and future risk assessment. In particular, Northern Europe will experience an increasing probability of concurring high sea level and heavy precipitation beyond the effects of mean SLR, caused mainly by more intense precipitation in a warmer climate. We have shown that ignoring the dependency in the occurrence of heavy precipitation and storm surges may underestimate the CF probability

in a warming climate by up to two orders of magnitude. Given the high cost of implementing flood risk reduction measures, these interventions require careful planning, supported by detailed flood risk assessments. Our study identifies the European regions potentially facing CF in a warmer future climate, thereby providing a continental-scale basis for follow-up local CF risk assessments and adaptation planning.

MATERIALS AND METHODS
Data
Storm surges were simulated with the DFLOW FM model using a flexible mesh setup (forced with 6-hourly wind and atmospheric pressure fields) (17, 20, 21, 29). Waves were simulated with the model Wavewatch III (17, 20, 22) (forced with a 6-hourly wind field). Astronomical tides were simulated every 6 hours using the FES2012 model (29, 31), which makes use of satellite altimetry data. The resulting sea level data are available every ~25 km along the coastline. Comprehensive validation and detailed information of the models can be found in (17, 20–22, 29). Our analysis was based on quantile values; therefore, we did not bias correct simulated data. Sea level and precipitation data were based on ERA-Interim and six selected models from the CMIP5 multimodel ensemble (i.e., ACCESS1-0, ACCESS1-3, GFDL-ESM2M, GFDL-ESM2G, CSIRO-Mk3-6-0, and EC-EARTH). CMIP5 models were selected on the basis of the skill in representing the synoptic climatologies and interannual variations across the northeast Atlantic region (17, 20–22). The GFDL-ESM2G model was not considered along the Black Sea coast because of instabilities of the surge model. Choosing well-performing CMIP5 models reduces the risk of artifacts caused by the delta change approach (27) (see below).

Precipitation was taken from the grid point nearest to each coastal location and, on each day, we considered accumulated precipitation within a time range of ±1 days. This choice allows for indirectly accounting for a range of large-scale weather systems that may produce CF. Grid point precipitation represents a rather large area of typically well beyond 100 km by 100 km. In a moving cyclone, precipitation at the daily scale is strongly correlated in space, and in particular, 3-day aggregated precipitation represents a large area quite far upwind. In addition, we accounted for very heavy precipitation falling in convective cells embedded in a large-scale weather system; these events would show up as heavy even in a 3-day aggregation and may cause CF in rather small catchments.

The effect of SLR on the astronomical tide was quantified through dynamic tidal ocean simulations (using the DFLOW FM model) (fig. S8). The simulations considered SLR scenarios resulting from the combination of steric changes with three land-ice scenarios of water contributions from ice sheets and glaciers (18). The analysis is described in detail in (17) with the only difference that we considered changes in the complete time series, rather than in the daily maxima only. Since the sensitivity of the final tide amplitude to the land-ice scenarios is very small (17), we considered the median of the three scenarios only. The actual observed time lag between the surge and astronomical tide sequences is random. The estimated CF return periods are thus just one random realization of all possible time lags between surges and astronomical tides. To get an estimate of a more likely CF return period, we computed the median of all possible estimates. We observe that this procedure does not allow one to take into account the variability of the return periods caused by the natural variability of the meteorological conditions. For the ERA-Interim–driven data, we obtained this estimate by calculating 240 individual estimates based on the superposition of (i)

the simulated surge time series (including waves) and (ii) the randomly shifted tide time series. The part of the tide series beyond the length of the surge series was moved to the start date. From this ensemble, we computed the median of the CF return periods (Fig. 2). It turned out that the difference between the standard estimate and the bootstrap-based estimate was small. As this procedure is computationally expensive, we therefore refrained from applying it to the CMIP5-based data.

Discussion about sea level modeling
The different sea level components were considered as independent in this study (i.e., SLR, astronomical tides, waves, and storm surges), and the only nonlinear interaction resolved was the effect of SLR on astronomical tides. This is an inevitable assumption for continental-scale studies due to the current computational, storage, and modeling capabilities. Astronomical tides and storm surges interact (28), and extreme sea levels occur during spring tides, the timing of which is to a large extent deterministic. However, as the timing of extreme weather events in a general circulation model is stochastic, coupled modeling would require several realizations of the same scenario to resolve the tidal modulation of weather driven of sea level extremes. Given that hydrodynamic models are computationally expensive, these simulations would not be feasible. The same limitation applies for resolving SLR effects on storm surge or waves (32). The multiple possible SLR trajectories would require repeating the simulations multiple times, which is computationally prohibitive, as would be the model resolution needed to resolve properly such interactions at European scale. In addition, recent studies have shown that the nonlinear effect of SLR on extreme sea levels also depends on the future shoreline dynamics (33), which is highly uncertain. Last, waves and currents also interact, but to our knowledge, there is no continental scale model that can simulate both processes in a coupled manner. The approach of considering the sea level components as independent is common in large-scale studies like the present (20, 34), and previous studies have demonstrated that the resulting errors are acceptable given the overall uncertainty of climate change projections (35, 36).

Statistical analysis
Return periods
There is no unique definition of CF return periods, with none of them being a priori superior. Each definition provides different information, and one should be chosen on the basis of the context and aim of the study (37). Here, the AND return period is chosen, which measures the probability of both individual hazards, sea level and precipitation, exceeding a chosen threshold. This definition allows for disentangling and understanding the dynamics of the potential flooding caused only by the concurrence of high sea level and precipitation values (1-year return levels). Specifically, we defined the bivariate CF return periods (26) as the mean waiting time between events where sea level and precipitation simultaneously exceed the individual 1-year return levels (i.e., the ~99.7th percentiles $s_{99.7}$ and $p_{99.7}$). To allow for a robust estimation, we applied a parametric copula-based bivariate probability distribution. Applying a parametric model for the full range of values, one would run the risk of biasing the representation of the extreme tail by the bulk of the bivariate distribution where most data occur. Therefore, we applied the model only to pairs of high values. We selected pairs where, simultaneously, sea level and precipitation values exceed the individual 95th percentiles (s_{sel} and p_{sel}, respectively). In a very few locations, one might end up with selecting few pairs only. Here, we reduced the selection threshold 0.95 to ensure that at least 20 pairs of values were selected

(never below 0.9). Clusters of selected event pairs separated by less than 3 days were replaced by a unique event, which assumed the maximum sea level S and precipitation P observed in the cluster (fig. S9).

The bivariate return period is thus given as

$$T(s_{99.7}, p_{99.7}) = \frac{\mu}{P((s > s_{99.7} \text{ and } p > p_{99.7}) | (s > s_{\text{sel}} \text{ and } p > p_{\text{sel}}))}$$

$$= \frac{\mu}{1 - u_{S99.7} - u_{P99.7} + C_{SP}(u_{S99.7}, u_{P99.7})} \quad (1)$$

where μ is the average time elapsing between the selected pairs, $u_{S99.7} = F_S(s_{99.7})$, F_S is the marginal cumulative distribution of the excesses over the selection threshold (accordingly for precipitation), and C_{SP} is the copula modeling the dependence between the selected pairs.

The marginal distributions of sea level and precipitation beyond the selection thresholds were modeled by a generalized Pareto distribution. Copulas were fitted to (u_S, u_P) [obtained via empirical marginal cumulative distribution function (CDF) (26)] and selected via Akaike information criterion from the families: Gaussian, t, Clayton, Gumbel, Frank, Joe, BB1, BB6, BB7, and BB8. Marginal distributions and copulas were fitted through a maximum likelihood estimator [via the ismev (38) and VineCopula (39) R-packages]. Goodness of fit of marginals and copulas was tested on the basis of the Cramer-von-Mises criterion (one-tailed; $N_{\text{boot}} = 100$ for copulas) [via the eva (40) and VineCopula (39) R packages, respectively]. The projected change (%) of the return period T was estimated for the individual CMIP5 models as $\Delta T(\%) = 100 \cdot (T^{2070-2099} - T^{1970-2004})/T^{1970-2004}$ (Fig. 3A and fig. S10).

Sampling uncertainty of ERA-Interim–based CF return periods
To obtain the 95% sampling uncertainty range of the ERA-Interim–based CF return periods in Fig. 3C, we applied a resampling procedure. The uncertainty was computed in the 11 representative locations whose return periods are shown in black in Fig. 3C. We based our estimate of sampling uncertainty on the previously generated 240 bivariate sea level/precipitation time series (where surge and precipitation are identical; only the astronomical tides were resampled). Each of these 240 bivariate time series were used for a further resampling procedure by combining bootstrapped numerator and denominator values of the return period expression (Eq. 1). The numerator-bootstrapped values of μ were obtained via resampling the observed times elapsing between the selected pairs (s_i, p_i) used for fitting the parametric probability density function (pdf); the denominator-bootstrapped values were obtained via resampling the observed pairs (s_i, p_i) used for the fit of the pdf. The final return period sampling uncertainty range was defined as the 2.5th to 97.5th percentile interval of the $240 \cdot 240$ return period estimates. This procedure is preferred to a classic resampling of all the pairs, which, here, would bias the obtained median return period due to the serial correlation of the sea level time series. On the basis of a large sample of data without any serial correlation, we estimated that the 95% sampling uncertainty range is overestimated by 30% from our procedure (with respect to a classic resampling procedure). Thus, conclusions about the detection of a climate change signal in the future (Fig. 3C) are conservative.

Delta change approach
We computed CF return periods for the future via the delta change approach (27), i.e., multiplying the ERA-Interim–based historical return period $T_{\text{Era}}^{1980-2004}$ by the individual CMIP5 model i variation of the CF return periods $T_{\text{Model } i}^{2070-2099} / T_{\text{Model } i}^{1980-2004}$. The present-day reference period is the intersection of the ERA-Interim and the historical CMIP5 data,

for which sea level simulations are available. See fig. S5 for comparing return periods based on ERA-Interim and individual CMIP5 models.

Attribution of return period variation
We carried out three experiments (3) to assess how the CF probability would change in future when only considering variation—with respect to the present—of (a) the dependence between sea level and precipitation, (b) the sea level overall marginal distributions (i.e., the distribution of the sea level without reference to precipitation), and (c) the precipitation overall marginal distribution. We estimated the relative change of the probability that would have occurred for experiment (i) as $\Delta_{\text{exp } i} = 100 \cdot (T_{\text{exp } i}^{\text{fut}} - T^{\text{pres}})/T^{\text{pres}}$ (Fig. 4), where T^{pres} is the return period for the present period and $T_{\text{exp } i}^{\text{fut}}$ is computed as follows. Experiment (a): Given the variables $(S_{\text{fut}}, P_{\text{fut}})$, we got the associated empirical cumulative distribution $(U_{S_{\text{fut}}}, U_{P_{\text{fut}}})$. From the variables S_{pres} and P_{pres}, we defined the empirical CDFs $F_{S_{\text{pres}}}$ and $F_{P_{\text{pres}}}$, through which we defined $S_a = F_{S_{\text{pres}}}^{-1}(U_{S_{\text{fut}}})$ and $P_a = F_{P_{\text{pres}}}^{-1}(U_{P_{\text{fut}}})$. The variables (S_a, P_a) have the same Spearman correlation and tail dependence (3) as $(S_{\text{fut}}, P_{\text{fut}})$, but marginal distributions as in the present period. We computed the return period $T_{\text{exp a}}^{\text{fut}}$ based on (S_a, P_a). Experiment (b): Given the variable S_{pres}, we got the associated empirical cumulative distribution $U_{S_{\text{pres}}}$. From the variable S_{fut}, we defined the empirical CDFs $F_{S_{\text{fut}}}$, through which we defined $S_b = F_{S_{\text{fut}}}^{-1}(U_{S_{\text{pres}}})$. The variables (S_b, P_{pres}) have the same Spearman correlation and tail dependence as during the present, but the marginal distribution of S_b is that of the future. We computed the return period $T_{\text{exp b}}^{\text{fut}}$ based on (S_b, P_{pres}). Experiment (c): as experiment (b), exchanging precipitation and sea level variables.

REFERENCES AND NOTES
1. S. I. Seneviratne, N. Nicholls, D. Easterling, C. M. Goodess, S. Kanae, J. Kossin, Y. Luo, J. Marengo, K. McInnes, M. Rahimi, A. Sorteberg, C. Vera, X. Zhang, Changes in climate extremes and their impacts on the natural physical environment, in *Managing the Risks of Extreme Events and Disasters to Advance Climate Change Adaptation. A Special Report of Working Groups I and II of the Intergovernmental Panel on Climate Change (IPCC)*, C. B. Field, V. Barros, T. F. Stocker, D. Qin, D. J. Dokken, K. L. Ebi, M. D. Mastrandrea, K. J. Mach, G. K. Plattner, S. K. Allen, M. Tignor, P. M. Midgley, Eds. (Cambridge Univ. Press, 2012), chap. 3, pp. 109–230.
2. T. Wahl, S. Jain, J. Bender, S. D. Meyers, M. E. Luther, Increasing risk of compound flooding from storm surge and rainfall for major US cities. *Nat. Clim. Chang.* 5, 1093–1097 (2015).
3. E. Bevacqua, D. Maraun, I. H. Haff, M. Widmann, M. Vrac, Multivariate statistical modelling of compound events via pair-copula constructions: Analysis of floods in Ravenna (Italy). *Hydrol. Earth Syst. Sci.* 21, 2701–2723 (2017).
4. P. J. Ward, A. Couasnon, D. Eilander, I. D. Haigh, A. Hendry, S. Muis, T. I. E. Veldkamp, H. C. Winsemius, T. Wahl, Dependence between high sea-level and high river discharge increases flood hazard in global deltas and estuaries. *Environ. Res. Lett.* 13, 084012 (2018).

5. R. M. Trigo, C. Ramos, S. S. Pereira, A. M. Ramos, J. L. Zêzere, M. L. Liberato, The deadliest storm of the 20th century striking Portugal: Flood impacts and atmospheric circulation. *J. Hydrol.* **541**, 597–610 (2016).

6. B. van den Hurk, E. van Meijgaard, P. de Valk, K.-J. van Heeringen, J. Gooijer, Analysis of a compounding surge and precipitation event in the Netherlands. *Environ. Res. Lett.* **10**, 035001 (2015).

7. D. Paprotny, O. Morales-Nápoles, S. N. Jonkman, HANZE: A pan-European database of exposure to natural hazards and damaging historical floods since 1870. *Earth Syst. Sci. Data* **10**, 565–581 (2018).

8. S. Pfahl, H. Wernli, Quantifying the relevance of cyclones for precipitation extremes. *J. Climate* **25**, 6770–6780 (2012).

9. C. Svensson, D. A. Jones, Dependence between sea surge, river flow and precipitation in south and west Britain. *Hydrol. Earth Syst. Sci.* **8**, 973–992 (2004).

10. J. Zscheischler, S. I. Seneviratne, Dependence of drivers affects risks associated with compound events. *Sci. Adv.* **3**, e1700263 (2017).

11. H. R. Moftakhari, G. Salvadori, A. AghaKouchak, B. F. Sanders, R. A. Matthew, Compounding effects of sea level rise and fluvial flooding. *Proc. Natl. Acad. Sci. U.S.A.* **114**, 9785–9790 (2017).

12. K. Kumbier, R. C. Carvalho, A. T. Vafeidis, C. D. Woodroffe, Investigating compound flooding in an estuary using hydrodynamic modelling: A case study from the Shoalhaven River, Australia. *Nat. Hazards Earth Syst. Sci.* **18**, 463–477 (2018).

13. P. J. Ward, B. Jongman, J. C. J. H. Aerts, P. D. Bates, W. J. W. Botzen, A. D. Loaiza, S. Hallegatte, J. M. Kind, J. Kwadijk, P. Scussolini, H. C. Winsemius, A global framework for future costs and benefits of river-flood protection in urban areas. *Nat. Clim. Chang.* **7**, 642–646 (2017).

14. W. Wu, K. McInnes, J. O'Grady, R. Hoeke, M. Leonard, S. Westra, Mapping dependence between extreme rainfall and storm surge. *J. Geophys. Res. Oceans* **123**, 2461–2474 (2018).

15. S. Pfahl, P. A. O'Gorman, E. M. Fischer, Understanding the regional pattern of projected future changes in extreme precipitation. *Nat. Clim. Chang.* **7**, 423–427 (2017).

16. Y. Hirabayashi, R. Mahendran, S. Koirala, L. Konoshima, D. Yamazaki, S. Watanabe, H. Kim, S. Kanae, Global flood risk under climate change. *Nat. Clim. Chang.* **3**, 816–821 (2013).

17. M. I. Vousdoukas, L. Mentaschi, E. Voukouvalas, M. Verlaan, L. Feyen, Extreme sea levels on the rise along Europe's coasts. *Earths Future* **5**, 304–323 (2017).

18. J. Hinkel, D. Lincke, A. T. Vafeidis, M. Perrette, R. J. Nicholls, R. S. Tol, B. Marzeion, X. Fettweis, C. Ionescu, A. Levermann, Coastal flood damage and adaptation costs under 21st century sea-level rise. *Proc. Natl. Acad. Sci. U.S.A.* **111**, 3292–3297 (2014).

19. S. Hallegatte, C. Green, R. J. Nicholls, J. Corfee-Morlot, Future flood losses in major coastal cities. *Nat. Clim. Chang.* **3**, 802–806 (2013).

20. M. I. Vousdoukas, L. Mentaschi, E. Voukouvalas, M. Verlaan, S. Jevrejeva, L. P. Jackson, L. Feyen, Global probabilistic projections of extreme sea levels show intensification of coastal flood hazard. *Nat. Commun.* **9**, 2360 (2018).

21. M. I. Vousdoukas, E. Voukouvalas, A. Annunziato, A. Giardino, L. Feyen, Projections of extreme storm surge levels along Europe. *Climate Dynam.* **47**, 3171–3190 (2016).

22. L. Mentaschi, M. I. Vousdoukas, E. Voukouvalas, A. Dosio, L. Feyen, Global changes of extreme coastal wave energy fluxes triggered by intensified teleconnection patterns. *Geophys. Res. Lett.* **44**, 2416–2426 (2017).

23. D. P. Dee, S. Uppala, A. Simmons, P. Berrisford, P. Poli, S. Kobayashi, U. Andrae, M. Balmaseda, G. Balsamo, P. Bauer, P. Bechtold, A. C. M. Beljaars, L. van de Berg, J. Bidlot, N. Bormann, C. Delsol, R. Dragani, M. Fuentes, A. J. Geer, L. Haimberger, S. B. Healy, H. Hersbach, E. V. Hólm, L. Isaksen, P. Kållberg, M. Köhler, M. Matricardi, A. P. McNally, B. M. Monge-Sanz, J.-J. Morcrette, B.-K. Park, C. Peubey, P. de Rosnay, C. Tavolato, J.-N. Thépaut, F. Vitart, The ERA-Interim reanalysis: Configuration and performance of the data assimilation system. *Q. J. Roy. Meteorol. Soc.* **137**, 553–597 (2011).

24. K. E. Taylor, R. J. Stouffer, G. A. Meehl, An overview of CMIP5 and the experiment design. *Bull. Am. Meteorol. Soc.* **93**, 485–498 (2012).

25. O. Martius, S. Pfahl, C. Chevalier, A global quantification of compound precipitation and wind extremes. *Geophys. Res. Lett.* **43**, 7709–7717 (2016).

26. S. Vandenberghe, N. Verhoest, C. Onof, B. De Baets, A comparative copula-based bivariate frequency analysis of observed and simulated storm events: A case study on Bartlett-Lewis modeled rainfall. *Water Resour. Res.* **47**, W07529 (2011).

27. D. Maraun, M. Widmann, *Statistical Downscaling and Bias Correction for Climate Research* (Cambridge Univ. Press, 2018).

28. T. Fernández-Montblanc, M. I. Vousdoukas, P. Ciavola, E. Voukouvalas, L. Mentaschi, G. Breyiannis, L. Feyen, P. Salamon, Towards robust pan-European storm surge forecasting. *Ocean Model.* **133**, 129–144 (2019).

29. S. Muis, M. Verlaan, H. C. Winsemius, J. C. Aerts, P. J. Ward, A global reanalysis of storm surges and extreme sea levels. *Nat. Commun.* **7**, 12913 (2016).

30. J. Zscheischler, S. Westra, B. J. J. M. Hurk, S. I. Seneviratne, P. J. Ward, A. Pitman, A. AghaKouchak, D. N. Bresch, M. Leonard, T. Wahl, X. Zhang, Future climate risk from compound events. *Nat. Clim. Change* **8**, 469–477 (2018).

31. D. Stammer, R. D. Ray, O. B. Andersen, B. K. Arbic, W. Bosch, L. Carrère, Y. Cheng, D. S. Chinn, B. B. Dushaw, G. D. Egbert, S. Y. Erofeeva, H. S. Fok, J. A. M. Green, S. Griffiths,

M. A. King, V. Lapin, F. G. Lemoine, S. B. Luthcke, F. Lyard, J. Morison, M. Müller, L. Padman, J. G. Richman, J. F. Shriver, C. K. Shum, E. Taguchi, Y. Yi, Accuracy assessment of global barotropic ocean tide models. *Rev. Geophys.* **52**, 243–282 (2014).

32. A. Arns, T. Wahl, S. Dangendorf, J. Jensen, The impact of sea level rise on storm surge water levels in the northern part of the German bight. *Coast. Eng.* **96**, 118–131 (2015).

33. J. Du, J. Shen, Y. J. Zhang, F. Ye, Z. Liu, Z. Wang, Y. P. Wang, X. Yu, M. Sisson, H. V. Wang, Tidal response to sea-level rise in different types of estuaries: The importance of length, bathymetry, and geometry. *Geophys. Res. Lett.* **45**, 227–235 (2018).

34. I. Losada, B. Reguero, F. Méndez, S. Castanedo, A. Abascal, R. Mínguez, Long-term changes in sea-level components in Latin America and Caribbean. *Glob. Planet Change* **104**, 34–50 (2013).

35. T. Howard, J. Lowe, K. Horsburgh, Interpreting century-scale changes in southern north sea storm surge climate derived from coupled model simulations. *J. Climate* **23**, 6234–6247 (2010).

36. R. Weisse, H. von Storch, H. D. Niemeyer, H. Knaack, Changing North Sea storm surge climate: An increasing hazard? *Ocean Coast. Manage.* **68**, 58–68 (2012).

37. F. Serinaldi, Dismissing return periods! *Stoch. Environ. Res. Risk Assess.* **29**, 1179–1189 (2015).

38. J. Heffernan, A. Stephenson, E. Gilleland, Ismev: An introduction to statistical modeling of extreme values. R package version 1.41 (2016).

39. U. Schepsmeier, J. Stoeber, E. C. Brechmann, B. Graeler, T. Nagler, T. Erhardt, Vinecopula: Statistical inference of vine copulas. R package version 2.0.5 (2016).

40. B. Bader, J. Yan, eva: Extreme value analysis with goodness-of-fit testing. R package version 0.2.4 (2016).

41. W. R. Peltier, D. F. Argus, R. Drummond, Space geodesy constrains ice age terminal deglaciation: The global ICE-6G_C (vm5a) model. *J. Geophys. Res. Solid Earth* **120**, 450–487 (2015).

42. E. Hertig, D. Maraun, J. Bartholy, R. Pongracz, M. Vrac, I. Mares, J. M. Gutiérrez, J. Wibig, A. Casanueva, P. M. M. Soares, Comparison of statistical downscaling methods with respect to extreme events over europe: Validation results from the perfect predictor experiment of the COST Action VALUE. *Int. J. Climatol.* **39**, 3846–3867 (2018).

43. M. R. Haylock, N. Hofstra, A. M. G. Klein Tank, E. J. Klok, P. D. Jones, M. New, A European daily high-resolution gridded data set of surface temperature and precipitation for 1950–2006. *J. Geophys. Res. Atmos.* **113**, D20119 (2008).

44. D. L. Codiga, *Unified Tidal Analysis and Prediction using the Utide Matlab Functions* (Graduate School of Oceanography, University of Rhode Island, Narragansett, RI, 2011).

Science Advances

Higher probability of compound flooding from precipitation and storm surge in Europe under anthropogenic climate change

E. Bevacqua, D. Maraun, M. I. Vousdoukas, E. Voukouvalas, M. Vrac, L. Mentaschi and M. Widmann

ARTICLE TOOLS	http://advances.sciencemag.org/content/5/9/eaaw5531
SUPPLEMENTARY MATERIALS	http://advances.sciencemag.org/content/suppl/2019/09/16/5.9.eaaw5531.DC1
REFERENCES	This article cites 38 articles, 3 of which you can access for free http://advances.sciencemag.org/content/5/9/eaaw5531#BIBL
PERMISSIONS	http://www.sciencemag.org/help/reprints-and-permissions

Use of this article is subject to the Terms of Service